PCCP

Accepted Manuscript

ROYAL SOCIETY OF CHEMISTRY

www.rsc.org/pccp

Journal Name

ARTICLE

Tight-Binding Quantum Chemical Molecular Dynamics Simulations for the Elucidation of Chemical Reaction Dynamics in SiC Etching with SF_6/O_2 Plasma

Received 00th January 20xx,
Accepted 00th January 20xx

DOI: 10.1039/x0xx00000x

www.rsc.org/

Hiroshi Ito, Takuya Kuwahara, Kentaro Kawaguchi, Yuji Higuchi, Nobuki Ozawa, Momoji Kubo*

We used our etching simulator [H. Ito et al., *J. Phys. Chem. C,* 2014, **118**, 21580-21588] based on tight-binding quantum chemical molecular dynamics (TB-QCMD) to elucidate SiC etching mechanisms. First, the SiC surface is irradiated with SF_5 radicals, which are the dominant etchant species in experiments, with the irradiation energy of 300 eV. After SF_5 radicals bombard the SiC surface, Si-C bonds dissociate, generating Si-F, C-F, Si-S, and C-S bonds. Then, etching products, such as SiS, CS, SiF_x, and CF_x (x = 1–4) molecules, are generated and evaporated. In particular, SiF_x is the main generated species, and Si atoms are more likely to vaporize than C atoms. The remaining C atoms on SiC generate C-C bonds that may decrease the etching rate. Interestingly, far fewer Si-Si bonds than C-C bonds are generated. We also simulated SiC etching with SF_3 radicals. Although the chemical reaction dynamics are similar to etching with SF_5 radicals, the etching rate is lower. Next, to clarify the effect of O atom addition on the etching mechanism, we also simulated SiC etching with SF_5 and O radicals/atoms. After bombardment with SF_5 radicals, Si-C bonds dissociate in a similar way to the etching without O atoms. In addition, O atoms generate many C-O bonds and CO_y (y = 1–2) molecules, inhibiting the generation of C-C bonds. This indicates that O atom addition improves the removal of C atoms from SiC. However, for a high O concentration, many C-C and Si-Si bonds are generated. When the O atoms dissociate the Si-C bonds and generate dangling bonds, the O atoms terminate only one or two dangling bonds. Moreover, at high O concentrations there are fewer S and F atoms to terminate the dangling bonds than at low O concentration. Therefore, few dangling bonds of dissociated Si and C atoms are terminated, and they form many Si-Si and C-C bonds. Furthermore, we propose that the optimal O concentration is 50–60% because both Si and C atoms generate many etching products producing fewer C-C and Si-Si bonds are generated. Finally, we conclude that our TB-QCMD etching simulator is effective for designing the optimal conditions for etching processes in which chemical reactions play a significant role.

1. INTRODUCTION

Silicon carbide (SiC) is a promising wide-gap semiconductor material because it has excellent properties such as high thermal conductivity, high elastic modulus, and low thermal expansion. Therefore, SiC is expected to be suitable for use in harsh environments, and its application in technologies and products is likely to contribute to solving energy problems and realizing the low carbon society.[1] Microelectromechanical systems and device technologies that use SiC are important, and their performance and manufacturing processes have been widely studied.[1-5] Plasma etching is frequently used for micro- and nanoscale patterning of SiC.[1-15] However, the bond between the silicon and carbon atoms in SiC is strong, making sculpting SiC difficult.[2] Therefore, for an optimal etching process it is important to maintain a high etching rate and decrease the deformation of etching holes.

Institute for Materials Research, Tohoku University, 2-1-1 Katahira, Aoba-ku, Sendai 980-8577, Japan. E-mail: momoji@imr.tohoku.ac.jp; Tel: +81-22-215-2050.

Plasma etching has been studied experimentally to develop a SiC etching technique. Kuah et al. etched poly-SiC, which contains different single-crystalline structures, with etchant gases such as CF_4 and SF_6.[3] They showed that SF_6 has a higher etching rate than CF_4. In recent studies, SiC etching has been performed with mixed etchant gases to improve the etching rate and processing accuracy. Tseng et al. performed 4H-SiC etching with NF_3 mixed with O_2 or HBr, and investigated the dependence of the etching rates and shape of etching holes on the composition of the etchant gases.[4] They concluded that the addition of O_2 to NF_3 gas increases etching rate, whereas HBr did not improve the accuracy of the etching process because tapered etching holes were generated. Fraga et al. etched a SiC thin film with a SF_6 etchant gas mixed with O_2.[5] They found that SF_5^+ and SF_3^+ are the first and second most commonly generated species in SF_6 plasma. During etching with SF_6/O_2 plasma, SiF_3, SiF, CO, CO_2, COF, and COF_2 were generated as etching products. The highest etching rate was achieved at an O_2 concentration of 20%. Recently,[1-3,5-15] mixtures of SF_6 and O_2 have been the most popular etchant gases for SiC etching because mixed etchant gases improve the etching rate. However, it is difficult to elucidate the etching mechanisms on an atomic scale experimentally and optimize the mixing rate. Although

the effect of several parameters, such as etchant species and gas composition[4-10] on etching rate has been investigated, the reasons why the etching rate depends on etchant species are still a matter of speculation. This is because experimental studies largely rely on heuristic analysis, and the chemical reaction dynamics on the SiC surface are unclear. To develop SiC etching techniques further, the atomic scale etching mechanisms must be investigated.

Computer simulations are suitable for investigating dynamic behavior in SiC etching on an atomic scale. Classical molecular dynamics (MD) methods have been used to investigate the effects of the impact of the etchant species and the etching yields.[16-19] Lu et al. simulated SiC etching with F^+ ions, and found that etching yield increases as the temperature of the SiC surface increases.[16] Prskalo et al. simulated SiC sputtering processes with Ar atoms, and demonstrated that increasing the incident energy of the Ar atoms increases the sputter yield.[18] These simulations analyzed the dynamic behaviors on a SiC surface on the atomic scale, and calculated the behavior of the atomic impact and the progression rate of the processes. In SiC etching, chemical reactions between the SiC surface and etchant species play a significant role in the dissociation of strong Si-C bonds. However, chemical reaction dynamics accompanying electron transfer is difficult to calculate by using classical MD method because it does not consider electrons. In contrast, static first-principles calculations can be used to simulate chemical reactions. Bui et al. performed density functional theory (DFT) calculations of the catalyst-referred etching of 3C-SiC.[19] They modeled the SiC surface terminated by –F and –OH groups and calculated activation barriers for the generation of a HF molecule from these groups. They revealed that generation occurs more readily at step edges on the SiC surface than that at terraces. First-principles calculations can provide the reaction paths of chemical reactions on SiC, which is important information for designing an optimal etching process. However, the static first-principles method cannot calculate the effects of velocity and impacts in SiC etching. Although first-principles MD can elucidate the effect of impact dynamics on chemical reactions, the computational cost of the method is huge and it has not been used to simulate SiC etching. Therefore, we developed a tight-binding quantum chemical molecular dynamics (TB-QCMD) method for investigating chemical reactions and electron transfer dynamics.[20-31] Our TB-QCMD code is more than 5000-fold faster than conventional first-principles MD methods and has already been used to investigate various chemical reaction processes, such as tribochemical reactions,[20] chemical vapor deposition of silicon,[21-23] the silica sol-gel process,[24] and the oxidation of CO in emission control catalysts.[25] Moreover, we developed an etching process simulator based on our TB-QCMD method[26,27] Our etching process simulator clarifies the effect of impact dynamics on chemical reactions during etching to reveal etching mechanisms on an atomic scale. In our previous paper, we simulated SiO_2 etching by CF_2 and CF_3 radicals, which are the dominant species in plasma-activated C_4F_8 and CF_4 gases.[27] We successfully simulated chemical reaction dynamics during the SiO_2 etching process, and clarified the effects of the etchant species and its irradiation energy on the etching rate.

In this paper, we use our TB-QCMD etching simulator to elucidate the mechanisms of SiC etching by SF_5 and SF_3 radicals, which are the dominant etchant species in SF_6 plasma.[5,32] We investigate chemical reaction dynamics between the SiC surface and etchant species. The effects of the chemical reactions on the progress of etching and the generation of etching products, and the bond formation on the SiC surface, are discussed. Moreover, to clarify the effect of O addition on SF_6/O_2 plasma etching of SiC,[1-3,5-15] we also simulate SiC etching with a mixture of SF_5 and O radicals/atoms. Further, we suggest an optimized mixing rate for etchant gases based on the simulation results. This is the first study to simulate SiC etching with two different etching species by using a quantum chemical MD method, discuss etching mechanisms on an atomic scale, and suggest the optimal composition of etchant species.

Table 1. Parameters for each atom for the TB-QCMD simulation. I is the ionization potentials from the valence orbital. ζ is the Slater-type atomic orbital exponent.

Atom	I (eV)[a]		ζ (Å^{-1})	
	s orbital	p orbital	s orbital	p orbital
H	13.598	-	1.24	-
C	24.376	11.257	1.72	1.72
O	35.115	13.617	2.25	2.25
F	34.968	17.422	2.55	2.55
Si	16.345	8.151	1.75	1.75
S	23.329	10.360	2.05	2.05

[a] Reference 36.

2. METHOD

In this study, we use our etching simulator based on TB-QCMD[33-35] to calculate the chemical reaction and electron transfer dynamics in SiC etching processes. Our simulator uses the following Hamiltonian:

$$H_{rs} = \frac{1}{2} K_{rs} S_{rs} \left(H_{rr} + H_{ss} \right) \quad (1)$$

$$K_{rs} = \left\{ 1 + \kappa_{rs} \left(1 - \Delta^4 \right) + \Delta^2 \right\} \exp\left[-\delta_{rs} \left\{ r_{rs} - \left(d_r + d_s \right) \right\} \right] \quad (2)$$

$$\Delta = \frac{H_{rr} - H_{ss}}{H_{rr} + H_{ss}} \quad (3)$$

where r_{rs} is the distance between the two atoms to which the molecular orbitals belong, d_r is the radius of each orbital, and κ_{rs} and δ_{rs} are positive empirical parameters. The diagonal matrix element, H_{rr}, is equal to the negative of the ionization potential for valence electrons, I_r; $H_{rr} = -I_r$. We use the ionization potentials of H, C, O, F, Si, and S atoms in reference 36. The off-diagonal term, H_{rs}, is calculated from equation 1, where S_{rs} is the overlap integral matrix. We use single-zeta Slater-type orbitals as atomic orbitals. The ionization potentials and zeta values are shown in Table 1. The parameters κ_{rs} and δ_{rs} are given in Table 2. These parameters are calculated to fit the Hamiltonian values of each orbital pair to those calculated by the *ab initio* method. The details of the fitting of Hamiltonian are shown in supporting information. The TB-QCMD employing the parameters in Table 2 shows good agreements in Hamiltonian matrix elements with

the Hartree-Fock calculations with STO-3G basis set. The total energy in the system is calculated with equations 4 and 5:

$$E = \sum_{i=1}^{N} \frac{1}{2} m_i v_i^2 + \sum_{k=1}^{OCC} \varepsilon_k + \sum_{i=1}^{N} \sum_{j>i}^{N} \frac{Z_i Z_j e^2}{R_{ij}} + \sum_{i=1}^{N} \sum_{j>i}^{N} E_{rep}(R_{ij}) \quad (4)$$

$$E_{rep}(R_{ij}) = b_{ij} \exp\left(\frac{a_{ij} - R_{ij}}{b_{ij}}\right) \quad (5)$$

In these equations, e is the elementary charge, R_{ij} is the internuclear distance, and a_{ij} and b_{ij} are parameters of the interaction between atoms i and j. a_{ij} and b_{ij} are related to the size and stiffness of atoms, respectively. The parameters a_{ij} and b_{ij} are shown in Table 3. Z_i is the atomic charge obtained by the electronic states calculations. Mulliken analysis[33,37] is used to obtain the value of Z_i. In equation 4, the first term is the kinetic energy of the atoms, the second term is the sum of the eigenvalues of all the occupied orbitals, and the third term is the Coulombic interaction. The last term corresponds to the short-range exchange-repulsion energy. To confirm the accuracy of the parameters a_{ij} and b_{ij}, we compare bond lengths of the TB-QCMD simulation with the experiments and first-principles methods in various molecules such as H_2, CH_4, H_2O, HF, SiH_4, H_2S, CO_2, CF_4, CS_2, O_2, F_2O, SO_2, F_2, SiF_4, SF_6, and S_8, and in various crystals such as diamond, silicon, silicon carbide, silicon dioxide, and silicon sulfide. The details of the comparison are summarized in supporting information (Table S1). The average differences in bond lengths between the TB-QCMD and other methods are 2.57% for the experiments, 2.66% for GGA PW91/DNP, 2.96% for LDA VWN/DNP, 3.88% for B3LYP/6-311G, 4.68% for MP2/6-311G, and 3.99% for HF/6-31G. These are almost the same as the difference between other methods such as 3.86% between the experiments and B3LYP, 5.38% between the experiments and MP2, 2.70% between GGA and B3LYP, 4.94% between LDA and MP2. The errors between the TB-QCMD and other methods are in the range of differences in the first-principles calculations depending on methods and basis sets. Therefore, the parameters a_{ij} and b_{ij} are acceptable for the etching simulation. Moreover, reaction energies of several chemical reactions are also described in supporting information (Table S2). The results are compared with other first-principles methods. In Table S2, the TB-QCMD results employing parameters in Tables 1-3 are in good agreement with them. Furthermore, to confirm the validity of the TB-QCMD by the comparison in the energy between the TB-QCMD and DFT, the time evolutions of energies during F and O atom irradiations are calculated and also shown in supporting information (Figs. S2 and S3). Figures S2 and S3 show the energy changes during F and O atoms are emitted to the SiC surface, respectively. In Figs. S2 and S3, the TB-QCMD simulations and static DFT calculations show that the energy has a peak just after the irradiation. This is because the emitted F and O atoms are very close to surface Si and C atoms by their collision. After that, the energy decreases to negative values (Figs. S2 and S3). This is because the emitted F and O atoms make bonds with Si and C atoms in the SiC structure. The TB-QCMD simulations show good agreement with the DFT calculations in energetic aspects. Therefore, the parameters in Tables 1-3 are sufficient to perform the SiC etching simulations. The atomic bond populations given by Mulliken population analysis[33,37] are calculated to clarify the bond-breaking,

Table 2. Parameters for each orbital pair for the TB-QCMD simulation.

Orbital pair					Parameters in TB calculation	
					κ_{rs}	δ_{rs}
H	(s)	-	H	(s)	0.84	0.001
H	(s)	-	C	(s)	1.22	0.24
H	(s)	-	C	(p)	1.34	0.12
H	(s)	-	O	(s)	1.39	0.24
H	(s)	-	O	(p)	1.56	0.26
H	(s)	-	F	(s)	1.86	0.28
H	(s)	-	F	(p)	1.70	0.001
H	(s)	-	Si	(s)	1.36	0.37
H	(s)	-	Si	(p)	1.28	0.01
H	(s)	-	S	(s)	1.45	0.28
H	(s)	-	S	(p)	1.58	0.25
C	(s)	-	C	(s)	1.30	0.24
C	(s)	-	C	(p)	1.76	0.45
C	(s)	-	O	(s)	1.33	0.29
C	(s)	-	O	(p)	2.24	0.52
C	(s)	-	F	(s)	1.94	0.45
C	(s)	-	F	(p)	2.51	0.99
C	(s)	-	Si	(s)	1.22	0.39
C	(s)	-	Si	(p)	1.59	0.34
C	(s)	-	S	(s)	1.43	0.29
C	(s)	-	S	(p)	1.89	0.43
C	(p)	-	C	(p)	1.95	0.002
C	(p)	-	O	(s)	1.86	0.31
C	(p)	-	O	(p)	2.43	0.00
C	(p)	-	F	(s)	2.62	0.63
C	(p)	-	F	(p)	2.57	0.001
C	(p)	-	Si	(s)	1.87	0.81
C	(p)	-	Si	(p)	2.07	0.001
C	(p)	-	S	(s)	2.07	0.39
C	(p)	-	S	(p)	2.41	0.001
O	(s)	-	O	(s)	1.49	0.38
O	(s)	-	O	(p)	2.21	0.40
O	(s)	-	F	(s)	1.91	0.44
O	(s)	-	F	(p)	2.53	0.61
O	(s)	-	Si	(s)	1.29	0.39
O	(s)	-	Si	(p)	1.65	0.34
O	(s)	-	S	(s)	1.52	0.38
O	(s)	-	S	(p)	2.01	0.40
O	(p)	-	O	(p)	2.79	0.22
O	(p)	-	F	(s)	2.69	0.43
O	(p)	-	F	(p)	2.55	0.001
O	(p)	-	Si	(s)	2.45	0.63
O	(p)	-	Si	(p)	2.47	0.001
O	(p)	-	S	(s)	2.48	0.52
O	(p)	-	S	(p)	2.99	0.12
F	(s)	-	F	(s)	2.36	0.70
F	(s)	-	F	(p)	3.21	0.80
F	(s)	-	Si	(s)	1.83	0.28
F	(s)	-	Si	(p)	2.39	0.30
F	(s)	-	S	(s)	1.91	0.44
F	(s)	-	S	(p)	2.67	0.43
F	(p)	-	F	(p)	2.65	0.24
F	(p)	-	Si	(s)	2.56	0.47
F	(p)	-	Si	(p)	2.59	0.001
F	(p)	-	S	(s)	2.58	0.57
F	(p)	-	S	(p)	2.61	0.001
Si	(s)	-	Si	(s)	1.50	0.37
Si	(s)	-	Si	(p)	2.03	0.36
Si	(s)	-	S	(s)	1.53	0.39
Si	(s)	-	S	(p)	2.43	0.41
Si	(p)	-	Si	(p)	2.19	0.11
Si	(p)	-	S	(s)	1.96	0.36
Si	(p)	-	S	(p)	2.49	0.001
S	(s)	-	S	(s)	1.63	0.38
S	(s)	-	S	(p)	2.31	0.39
S	(p)	-	S	(p)	2.83	0.21

Table 3. Parameters of each atom pair for the TB-QCMD simulation.

Atom pair	a_{ij}	b_{ij}
H - H	1.33	0.148
H - C	1.75	0.150
H - O	1.86	0.158
H - F	1.86	0.158
H - Si	2.19	0.163
H - S	2.13	0.160
C - C	2.32	0.149
C - O	2.21	0.157
C - F	2.32	0.157
C - Si	2.69	0.165
C - S	2.59	0.160
O - O	2.20	0.157
O - F	2.25	0.157
O - Si	2.68	0.165
O - S	2.49	0.165
F - F	2.36	0.165
F - Si	2.50	0.165
F - S	2.50	0.165
Si - Si	3.13	0.160
Si - S	2.89	0.160
S - S	2.87	0.160

bond-formation, and electron-transfer dynamics quantitatively during the chemical reactions. The atomic bond population, M_{XY}, is calculated by

$$M_{XY} = 4\sum_{r}^{\mathrm{onX}}\sum_{s}^{\mathrm{onY}}\sum_{j}^{OCC} C_{jr} C_{js} S_{rs} \quad (6)$$

where C_{jr} is the eigenvector element.

A schematic of the etching simulator is shown in Fig. 1. In the TB-QCMD etching simulator, the total number of atoms in the system can be changed by the appearance of the etchant species and the disappearance of vaporized molecules during etching simulations. These functions model the continuous irradiation by etchant species. The disappearance of vaporized molecules decreases the computational cost. In our previous study,[27] the etching conditions, such as the emission time interval, incident velocity, rotation, number, and elements of the etchant species, and the substrate temperature, could be changed. However, the previous etching simulator could handle only irradiation with a single species. Therefore, it cannot simulate SiC etching with SF_6/O_2 plasma. In this study, we develop an etching simulator that represents etching with two etchant species at an arbitrary ratio. Two different etchant species can be used with an inputted ratio, and the order of the irradiation species is randomly determined. Thus, our new etching simulator can investigate etching processes that are more complex and involve mixtures of gases. Therefore, this new function enables us to unravel the mechanisms and efficiency of complex etching processes with two etching species, and to predict the optimal ratio of gases.

In this study, we use a 4H-SiC crystal as an etching substrate. This is because crystalline SiC model is frequently employed in the simulation studies.[17-19] In particular, 4H-SiC has advantages in band gap and electron drift mobility,[38] and are mainly used in recent experimental studies.[4,9] Moreover, $(000\bar{1})$ surface has a great expectation because it has advantages in the growth rate[38] and the

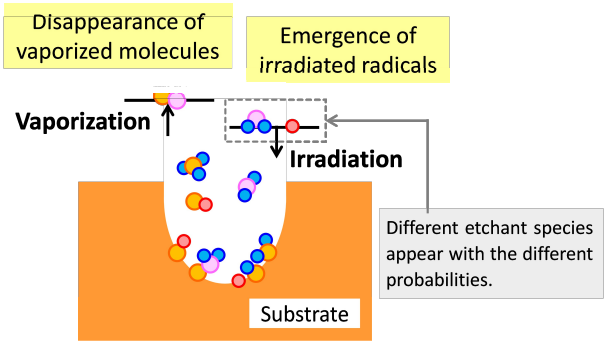

Figure 1. Schematic of our TB-QCMD etching simulator.

oxidation rate which are essential to fabricate the metal-oxide-semiconductor (MOS) interface.[4] Then, we performed the SiC etching simulations with 4H-SiC$(000\bar{1})$ surface. The top and bottom layers of the SiC surface are terminated with hydrogen atoms. The SiC surface consists of 360 atoms (H: 36; C: 162; Si: 162). The simulation cell contains a 16.0 × 9.2 Å *xy* plane parallel to the surface and a 60.0 Å *z*-axis perpendicular to the surface. The bottom 54 atoms (H: 18; C: 18; Si: 18) of the SiC substrate are fixed. The simulations are performed at 300 K. The temperature is controlled by scaling the atom velocities every 20 steps. In our etching simulations, we tried to reveal the elementary reaction for the etching progress. Therefore, the simple conditions are employed. Just before the irradiation begins, the etchant S atoms of SF_5 and SF_3 radicals and O atoms are randomly located in an area of 8.0 × 4.6 Å at the center of the *xy* plane, 9.7 Å above the SiC surface. SF_3 and SF_5 radicals are randomly rotated when they appear, however, the rotation energy is not supplied to them. The irradiation energy is assigned to the etchant radicals only in the *z* direction, and then etchant species are perpendicularly emitted onto the SiC surface. The vaporized molecules generated by the chemical reactions are automatically removed from the simulation cell after they reach a *z* position greater than 11.5 Å from the surface. The Verlet algorithm[39] is used for calculating atomic motion with a time step of 0.05 fs under three-dimensional periodic boundary conditions. The Ewald method[40] is used to calculate the Coulombic interactions. In the experimental etching, etchant species are generated from plasma-enhanced etchant gases. An electric field is applied, and ions are accelerated. Then, the substrate surface is mainly irradiated with ions such as SF_5^+, SF_3^+, and O^+.[5,41] When ions approach the substrate surface, ions trap electrons from the substrate material because of an energy stabilization of an electric field near an ion. Then, ions are neutralized near the substrate surface. This phenomenon is known as Auger neutralization.[42] Therefore, the simulation on the bombardment of neutralized species onto the substrate surface represents the experimental etching process. In fact, in the etching simulations based on classical molecular dynamics method, neutral species are used for the etching although those are described as "ions" for the discrimination from non-accelerated species.[46] As with the previous study, neutral species of SF_5, SF_3, and O radicals/atoms are used as etchant species in the present study. Twenty etchant radicals, consisting of SF_3, SF_5, or a mixture of SF_5 and O radicals/atoms, are sequentially irradiated at 0.60 ps intervals, starting at 0.30 ps. The

interval time is determined from our previous etching simulations[27] and similar studies based on classical MD.[43,44] In our previous study of SiO_2 etching by CF_2 and CF_3 radicals, an interval time of 0.50 ps was used, and the validity of the interval time already has been confirmed.[27] In the simulations, the atoms of the etchant species are not included in the temperature control until after the next etchant species appears. The vaporized molecules from the SiC surface are also removed from the temperature control. Moreover, in the experimental studies, the bias voltage controls the kinetic energy of the etchant species.[5,14,15] In fact, when rf bias is used, the distribution of generated ion energy is detected experimentally.[45] However, for the simulation study, it is very difficult to consider an energy distribution of ions because the number of ions is much smaller than experiments. In most of the etching simulation studies based on molecular dynamics methods, a constant irradiation energy is employed for monovalent positive ions through a simulation.[16,46] This is based on a simple time-averaged system in rf bias,[45] and in this system the kinetic energy of etchant species are defined as the multiplication of the ionic valence and the bias voltages. For example, when 200 V is forced on a monovalent positive ion, its energy is 200 eV.[45] In this study, an irradiation kinetic energy of 300 eV is used for the SF_5, SF_3, and O radicals/atoms, based on experimental studies, which used bias voltages of 300 V[10] and 60-700 V.[8,12,15] The kinetic energy of 300 eV corresponds to velocities of 21.346, 25.496, and 60.153 km/s for the SF_5, SF_3, and O radicals/atoms, respectively.

3. RESULTS AND DISCUSSIONS

A. SiC etching simulation with continuous irradiation of SF_5 and SF_3 radicals

Our TB-QCMD etching simulator is used to investigate chemical reaction dynamics during SiC etching by SF_5 and SF_3 radicals, which are the first and second most commonly generated species in SF_6 plasma.[5] First, we simulated the SiC etching with 20 SF_5 radicals at an irradiation energy of 300 eV. Fig. 2 shows snapshots of the simulation. The first SF_5 radical appears above the SiC surface, and hits the SiC surface at 0.35 ps (Figs. 2a and b). The S-F bonds of the SF_5 radicals are dissociated by the bombardment. The S and F atoms react with C and Si atoms on the SiC surface (Fig. 2c), producing C-S, C-F, and Si-F bonds, and the SiF molecules that are generated evaporate. After the fourth SF_5 bombardment, Si-S and H-F bonds are formed, and SiS and HF molecules are generated and evaporate (Fig. 2d). In the simulation, etching products containing Si atoms, such as SiF_x (x = 1–4) and SiS, are easier to form than those containing C atoms. In Fig. 2d, C-C bonds, which are detected experimentally,[8,13] are also generated on the SiC surface. During the simulation, Si atoms are removed by the generation of etching products, such as SiF_x and SiS, and many C atoms remain on the SiC surface, generating C-C bonds that also stay on the SiC surface. At 4.45 ps, a SiF_2 molecule is also generated and evaporated (Fig. 2e). Some F atoms penetrate the deep layers of the SiC substrate. After S-F bonds of SF_5 radical are dissociated by the

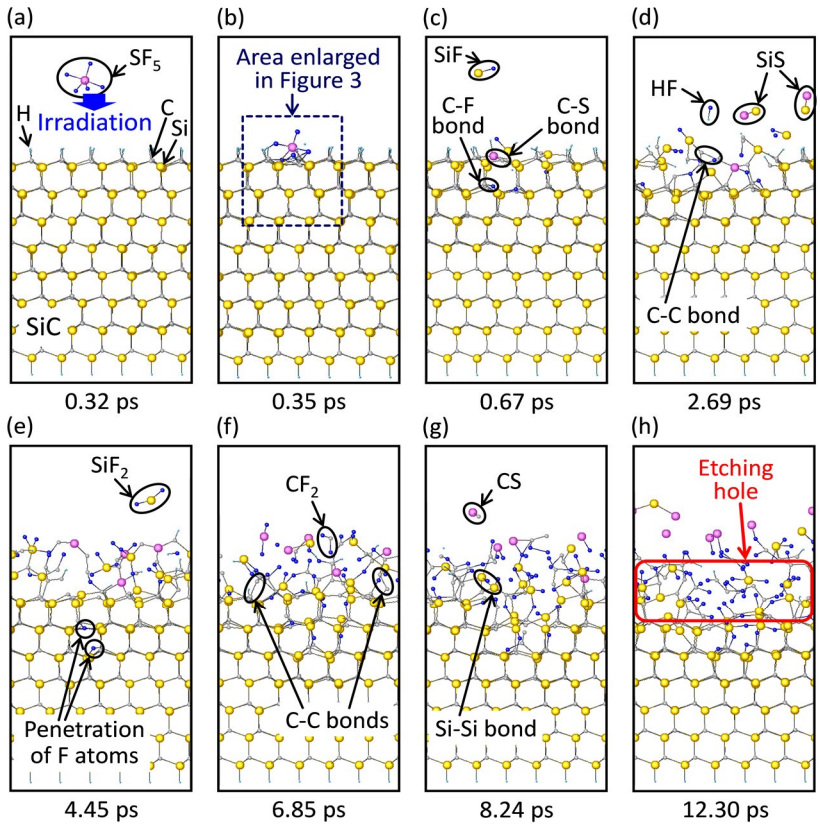

Figure 2. Snapshots of the simulation of SiC etching by SF_5 radicals (a) just after the first SF_5 radical irradiation, (b) during bombardment by the first SF_5 radical, and after the (c) first, (d) fourth (e) seventh, (f) 11th, (g) 14th, and (h) 20th SF_5 radical irradiation.

bombardment, the dissociated F atoms which have surplus kinetic energy can penetrate the SiC structure. Moreover, CF_2 and CS molecules are observed and evaporated at 6.85 and 8.24 ps, respectively (Figs. 2f and g). These results suggest that both S and F atoms contribute to removing Si and C atoms. In addition to the generation of C-C bonds on SiC, a Si-Si bond is also generated in Fig. 2g. Si-Si bonds and C-C bonds remain at the SiC surface. However, far fewer Si-Si bonds are generated than C-C bonds. This is because Si atoms are more likely to generate SiF_x and SiS molecules, and thus many Si atoms are removed by the vaporization of SiF_x and SiS molecules (Figs. 2c–e). In contrast, the remaining C atoms generate many C-C bonds and form clusters on the SiC surface (Figs. 2d and f). Finally, after the irradiation of 20 SF_5 radicals, many Si-C bonds are dissociated on the SiC surface (Fig. 2h). During the simulation, many C-C bonds are generated, and five-membered rings of C atoms are intermediately generated. This indicates that graphene-like structure can grow. For the investigation of C-C bond growth, there are the interesting studies such as the carbide-derived carbons (CDC)[47] and the pentagon-first mechanism[48]: The former study shows that carbon materials are formed from various carbide precursors by the removal of extra atoms in them via physical and chemical processes, and the latter shows the formation mechanism of five-membered ring of C atoms in the result of the oligomerization and the cross-linking reactions with a Fe cluster. In particular, V. Presser et al. reports the CDC technique of the formation of the graphene-like structure via the removing process of Ti and Si atoms from $Ti_xSi_yC_z$ materials by chemical reactions with Cl_2.[47] Comparison in the structures generated by C atoms, the formation of graphene-like structure in the TB-QCMD is similar as the CDC although the TB-QCMD shows just the initial stage of that. Moreover, SiS, CS, HF, SiF_x, and CF_x (x = 1–4) molecules are generated and evaporated. In experimental studies, SiF_x and CF_x molecules are the major etching products in SiC etching with SF_6 plasma.[15] Therefore, our simulation agrees with the experimental observations. However, etching products containing S atoms and S atom behavior have not been clearly-understood experimentally. In the simulation, S atoms react with Si and C atoms, generating SiS_y and CS_y (y = 1-2) molecules. Thus, our simulations successfully create the etching products that contain S atoms. After the SiC etching simulation, the surface consists of various atoms, including irradiated S and F atoms, and various bonds, such as Si-Si, C-C, and Si-C bonds (Figs. 2d, f, and g). There are many C atoms on the SiC surface, and it resembles an amorphous structure (Fig. 2h). These observations agree with experimental SiC etching, during which a non-crystalline, carbon-rich layer is formed on the SiC surface.[15] Our TB-QCMD etching simulator revealed chemical reaction dynamics, surface structure, and etching products on an atomic scale that could not be observed experimentally. Therefore, our results help to elucidate the etching mechanism.

During SiC etching, the generation of bonds and etching products is closely related to the chemical reaction dynamics of the etchant atoms. To reveal the chemical reaction dynamics in SiC etching, we calculate the atomic bond populations[27] during the first SF_5 irradiation, and analyze the bond formation and dissociation processes. Figs. 3a-c show scaled-up snapshots of the simulation in Fig. 2 from 0.35 to

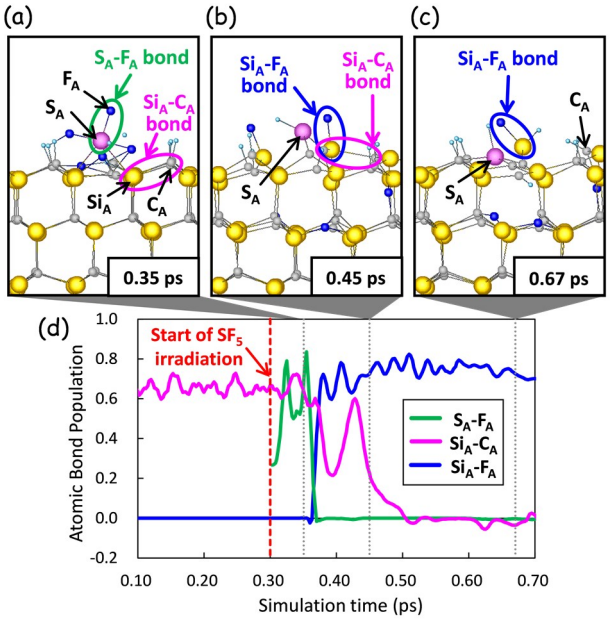

Figure 3. Time evolution of the atomic bond population of S_A-F_A, Si_A-C_A, and Si_A-F_A bonds. Insets show scaled up snapshots of the SiC etching by SF_5 radical at (a) 0.35, (b) 0.45, and (c) 0.67 ps.

0.67 ps. These snapshots show the dissociation of the S_A-F_A and Si_A-C_A bonds and formation of the Si_A-F_A bond. Before the reaction, the S_A and F_A atoms belong to the SF_5 radical, and the C_A and Si_A atoms are bound at the SiC surface. Fig. 3d shows the time evolution of the atomic bond population for the S_A-F_A, Si_A-C_A, and Si_A-F_A atom pairs. The first SF_5 radical appears on the SiC surface at 0.30 ps. The S_A-F_A atomic bond population changes from 0.3 to 0.8 (Fig. 3d) because of the vibration of the SF_5 radical. At 0.35 ps, the SF_5 radical reaches the SiC surface (Fig. 3a), and then the S_A-F_A and Si_A-C_A atomic bond populations are about 0.8 and 0.6, respectively (Fig. 3d). Therefore, these atom pairs form bonds. At 0.36 ps, the S_A-F_A atomic bond population decreases from 0.8 to 0.0 (Fig. 3d), indicating that the S_A-F_A bond is dissociated. At 0.37 ps, the Si_A-F_A atomic bond population increases from 0.0 to 0.7. The dissociated F_A atom forms bonds with the Si_A atom. At 0.40 ps, the Si_A-C_A atomic bond population temporarily decreases from 0.6 to 0.2, and this bond weakens. This indicates that the Si_A atom is still moved by the aftereffects of the bombardment, and temporarily approaches other atoms. At 0.45 ps, the Si_A-F_A and Si_A-C_A atomic bond populations are 0.7 and 0.2, respectively (Fig. 3d), and Si_A-F_A and Si_A-C_A bonds are observed (Fig. 3b). After 0.45 ps, the Si_A-C_A atomic bond population decreases to 0.0 in Fig. 3d. The Si_A-C_A bond is dissociated, and only the Si_A-F_A bond is detected at 0.67 ps (Fig. 3c). The irradiation of the SF_5 radical induces chemical reactions such as bond dissociation and bond formation. These reactions are promoted by the kinetic energy of etchant atoms.

Next, to reveal the chemical reaction dynamics in SiC etching by SF_3 radicals and to investigate the effects of the etchant species, we simulate SiC etching with 20 SF_3 radicals. Fig. 4 shows snapshots of the simulation of SiC etching with SF_3 radicals at an irradiation energy of 300 eV. The etching simulation conditions are the same for the etching simulation with SF_5 radicals. The SiC surface is continuously

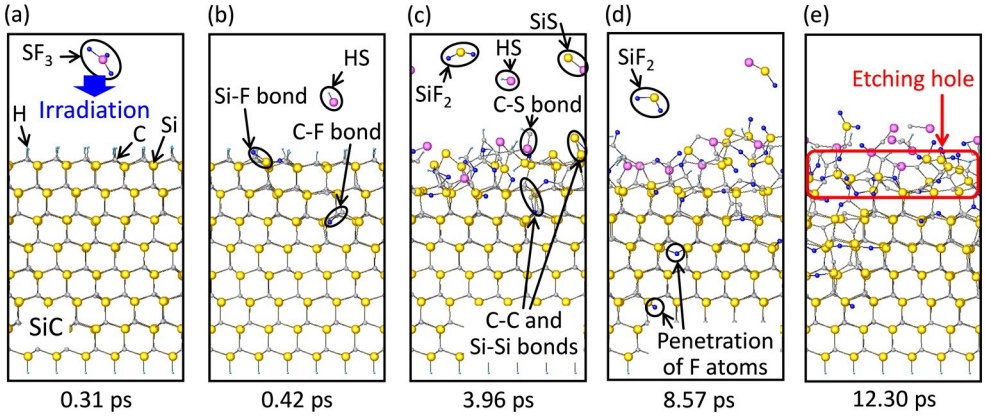

Figure 4. Snapshots of SiC etching simulation by SF_3 radicals (a) during the first SF_3 radical irradiation, and after the (b) first, (c) seventh, (d) 14th, and (e) 20th SF_3 radical irradiations.

irradiated with 20 radicals at 0.60 ps intervals. After the first SF_3 radical irradiation (Fig. 4a), S-F bonds of the SF_3 radical are dissociated, and S-H, Si-F, and C-F bonds are generated (Fig. 4b). Then, a HS molecule is generated and vaporized. These are similar chemical reactions to those observed for etching with SF_5 radicals. After the seventh SF_3 irradiation, Si-S and C-S bonds are generated, and SiS, SiF_2, and HS molecules are vaporized (Fig. 4c). Moreover, C-C and Si-Si bonds are generated and remain on the SiC surface. This bond generation is also observed in the simulation with SF_5 radicals, and it agrees with the results of experimental studies.[8,13] At 8.57 ps, a SiF_2 molecule is also generated and vaporized, and the penetration of irradiated F atoms is observed (Fig. 4d). A F atom of the SF_3 radical has a larger kinetic energy per atom than that of the SF_5 radical. Therefore, F atoms easily penetrate the SiC layers during etching with SF_3 radicals. On the other hand, S atoms are unlikely to penetrate the SiC surface. This is because a penetration of S atom requires the dissociation of three or five S-F bonds of SF_3 and SF_5 radicals. Moreover, S is a larger atom than a F atom, and then a higher energy barrier probably exists for a penetration of S atom than that of F atom. Finally, after 20 SF_3 irradiations, Si-C bonds at the surface are dissociated (Fig. 4e). In Fig. 4e, deformation of SiC structure is also observed at deep SiC layers as a result of a large number of F atom penetrations. The more F atoms penetrate the SiC surface, the fewer F atoms react with surface Si and C atoms. Penetrating F atoms form Si-F or C-F bonds in a deep SiC layer. Therefore, during etching with SF_3 radicals, more Si and C atoms remain on the SiC surface than during etching with SF_5 radicals (Figs. 2h and 4e). Hence, SiC etching with SF_3 radicals is expected to be slower than etching with SF_5 radicals. SF_3 and SF_5 radicals show differences in the number of Si and C atoms remaining on the surface and the penetration of F atoms, although the chemical reactions between SiC and the etchant species are similar.

To compare the effects of the etchant species on the chemical reactions in the SiC surface in detail, we calculated the numbers of Si-C, Si-F, and C-F bonds during the simulations (Fig. 5). These numbers reflect the probabilities of chemical reactions during the SiC etching. The number of bonds between two atoms is calculated by the atomic bond population. An atom pair that has an atomic bond population of more than 0.1 is defined as a bond. The numbers are calculated at the start, after each irradiation, and at the end of the simulations. The data for five simulation runs are averaged, and the error bars are also shown. Fig. 5a shows the variation in the numbers of Si-C bonds. During SF_5 radical etching, the number of Si-C bonds decreases more rapidly than during SF_3 radical etching. Therefore, the SF_5 radical dissociates many Si-C bonds increasing the etching rate. Figs. 5b and c show the number of generated Si-F and C-F bonds, which increase in both the SF_5 and SF_3 radical simulations. This indicates that the F atoms in the SF_5 and SF_3 radicals form bonds with the Si and C atoms in SiC. The SF_5 radical generates larger numbers of Si-F and C-F bonds than the SF_3 radical because the SF_5 radical has more F atoms, and thus makes a larger contribution to the generation of SiF_x molecules than the SF_3 radical does (Figs. 2c and e). More Si-F bonds than C-F bonds form during etching with SF_5 and with SF_3 radicals (Figs. 5b and c). This suggests that the Si atom is more likely to form bonds with F atoms than C atoms. Therefore, Si atoms are more likely to generate etching products, such as SiF_x molecules, than are C atoms because of the binding energy of the bonds. In the DFT calculations, the binding energies of Si-F and C-F bonds are 148.6 and 132.4 kcal/mol in SiF_4 and CF_4 molecules, respectively. Therefore, more SiF_x molecules are generated than CF_x molecules in the simulations (Figs. 2 and 4). In contrast, C atoms remain on the SiC surface, and C-C bonds are generated (Figs. 2d, 2f, and 4c). The more Si atoms are removed, the more C atoms remain. More C-C bonds are generated by etching with SF_5 than by etching with SF_3 radicals because the number of Si-F bonds generated increases with the number of F atoms. Finally, we confirm that SF_5 radicals dissociate more Si-C bonds and generate more etching products, and thus have a higher etching rate than SF_3 radicals.

B. Effect of the O addition on SiC etching process

During the SiC etching simulations with SF_5 and SF_3 radicals (Figs. 2 and 4), many C-C bonds and a few Si-Si bonds are generated. To compare the binding energy between C-C and Si-Si bonds, we calculated the energies of SiC surfaces whose C and Si atoms are

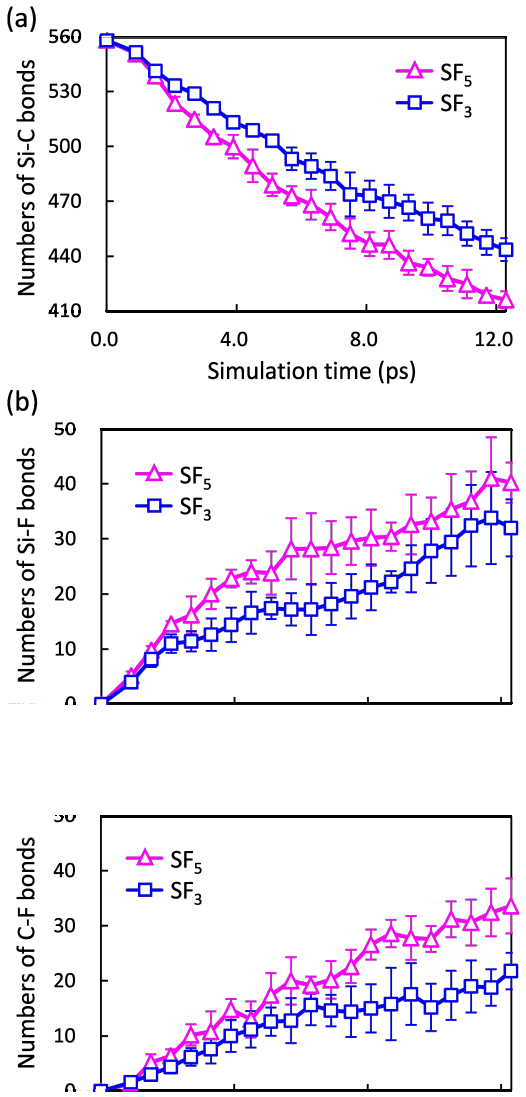

Figure 5. Time evolution of the number of (a) Si-C, (b) Si-F, and (c) C-F bonds during SiC etching simulations. Averaged data are shown for five simulation runs, and error bars indicate standard deviation.

terminated by -CH_3 and -SiH_3 groups, respectively. The calculation models are shown in supporting information (Fig. S4). In the TB-QCMD, a C-C bond on the SiC surface has a larger binding energy than a Si-Si bond for 18.9 kcal/mol. This is almost the same as those of the first-principles calculations such as 18.7 kcal/mol in GGA PW91/DNP and 24.3 kcal/mol in LDA VWN/DNP which are performed by Accelrys DMol^3 code.[49] This indicates that C-C bonds are likely to keep during the etching process. To remove C atoms from the SiC surface effectively, the etchant gas composition has been studied experimentally for SF_6/O_2 plasma.[1-3,5-15] However, the atomic scale mechanism of the chemical reaction dynamics of O atoms is still unclear. It is necessary to understand the etching mechanism of the SF_6/O_2 plasma process in order to optimize the etchant gas composition. Therefore, we also perform SiC etching simulations with combinations of SF_x and O radicals/atoms. We use the SF_5 radical because it has been identified experimentally as a dominant etchant species in SF_6/O_2 plasma.[5,32] The total number of irradiation species is 20. The ratio of O atoms to the total number of radicals is defined as an O concentration. We performed SiC etching simulations with SF_5 radicals and O atoms at O concentrations of 10–75%. During the simulations, the order of irradiation species is randomly determined. The irradiation energy of the etchant species is 300 eV, and the other simulation conditions are same as for SiC etching with SF_5 and SF_3 radicals.

Fig. 6 shows snapshots of the SiC etching simulation with SF_5 and O radicals/atoms at an O concentration of 50%. A SF_5 radical is randomly chosen as the first irradiated etchant species. In Fig. 6a, S-F and Si-C bonds dissociate, C-S, Si-F, C-F, and H-F bonds are generated, and HF and CS molecules are vaporized. At 1.51 ps, the SiC surface is irradiated with the first O atom, which is the third etchant species in this simulation (Fig. 6b). The irradiation of the second and third O atoms is also simulated (Fig. 6c). The O atoms form Si-O and C-O bonds at the SiC surface. These bonds are not generated during etching with SF_5 or SF_3 radicals (Figs. 2 and 4). Moreover, in the same snapshot, CS and CO molecules are generated and evaporated. CS molecules are also observed as etching products in the SiC etching without O atoms (Fig. 2), whereas CO molecules are only generated by O atom irradiation, and the etching products are different. The generation of CO molecules has also been observed experimentally,[5,8,13] demonstrating that the chemical reactions of O atoms are successfully simulated. After the SiC surface is irradiated with three SF_5 and five O atoms (Fig. 6d), O atoms penetrate the deep layers of the SiC. O atoms have higher kinetic energy than those of dissociated F atoms, and then easier to penetrate the SiC surface than F atoms in the etching by only SF_5 or SF_3 radicals. The O atoms form bonds with Si and C atoms, and do not evaporate immediately as molecules. In Figs. 6c and d, C-C and Si-Si bonds are observed. However, there are fewer C-C and Si-Si bonds than in the SiC etching simulations with SF_5 and SF_3 radicals (Figs. 2 and 4). During experimental SiC etching with SF_6/O_2 plasma, the likelihood of the carbon passivation layer forming decreases as the O_2 concentration increases.[12] Therefore, the simulation agrees with the experimental observations. C-C bonds are unlikely to form because O atoms remove C atoms from the SiC surface by generating CO molecules. After the irradiation of 10 SF_5 and 10 O radicals/atoms, the vaporization of CS and SiF molecules is also observed (Fig. 6e), and many Si-C bonds are dissociated. SiC etching by SF_5 and O radicals/atoms is successfully simulated..

We now compare the SiC etching simulations at different O concentrations. Figs. 7a–c shows snapshots of the etching simulations with 20 SF_5 or O radicals/atoms at O concentrations of 25%, 50%, and 75% at 12.30 ps. During etching at an O concentration of 25%, the SF_5 radical dissociates many Si-C bonds (Fig. 7a). In Fig. 7a, generation of Si-F, C-F, Si-S, and C-S bonds and the vaporization of SiF and CS molecules are observed. During the simulation, Si-O and C-O bonds are generated; however, many C atoms remain on the SiC, and C-C bonds form. At an O concentration of 50%, Si and C atoms form bonds

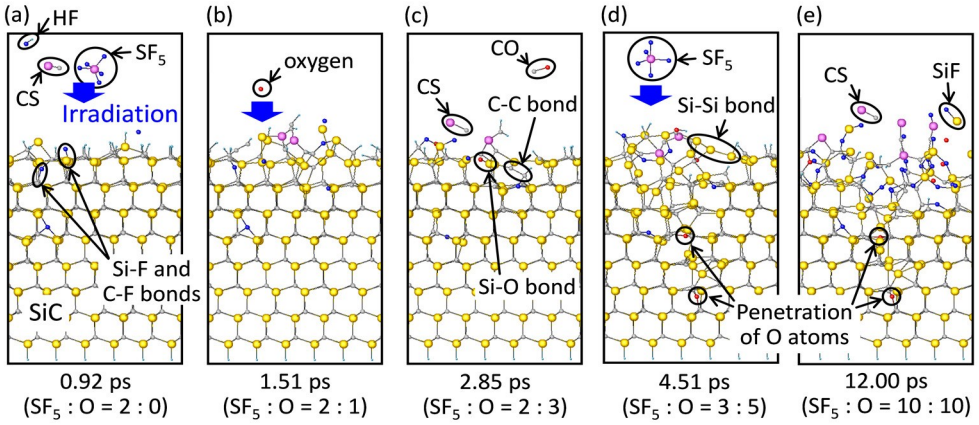

Figure 6. Snapshots of the simulation the SiC etching by both SF_5 and O radicals after irradiation with (a) two SF_5, (b) two SF_5 and an O, (c) two SF_5 and three O, (d) three SF_5 and five O, and (e) 10 SF_5 and 10 O radicals. The number of irradiated SF_5 and O radical is also indicated under each snapshot and simulation time.

with F, S, and O atoms (Fig. 7b). The O atom penetrates deep SiC layers, and forms many Si-O and C-O bonds. C-C bonds are also generated on the SiC surface. In the snapshot at an O concentration of 75%, penetration of O atoms is also observed (Fig. 7c). In addition to the dissociation of Si-C bond, C-C bonds are also generated on the SiC surface as well as etching at O concentrations of 25% and 50%. Interestingly, many Si-Si bonds are generated in addition to C-C bonds at an O concentration of 75%. During the simulation, Si-C bonds dissociate just after the irradiated radicals bombard the SiC surface, generating dangling bonds on these Si and C atoms. Just after radical irradiation, an O atom terminates only one or two dangling bonds of the Si and C atoms, although a SF_5 radical can terminate more than five dangling bonds. As the O concentration increases, the number of irradiated SF_5 radicals decreases instead of the number of O atoms increasing. Therefore, at high O concentrations, fewer dangling bonds are terminated than at low concentrations. At an O concentration of 75% (Fig. 7c), there are fewer S and F atoms to terminate the dangling bonds of dissociated Si and C atoms than at low O concentrations (Figs. 7a and b). The dissociated Si and C atoms form bonds with other Si and C atoms that have a dangling bond before they are terminated by the irradiated atoms. The generation of many Si-Si and C-C bonds may also decrease the etching rate and indicate the inefficient removal of Si and C atoms from the SiC. Therefore, etching with too many O atoms decreases the etching rate. Next, we focus on the penetration of O atom. At O concentrations of 50% and 75%, O atoms penetrate deep SiC layers (Figs. 7b and c). The penetrating O atoms do not react with the surface Si and C atoms, and form bonds with Si and C atoms in a deep layer. The SiC etching at high O concentrations increases the penetration of O atoms and then makes the etching process inefficient, preventing the generation of etching products. Based on the generation of Si-Si and C-C bonds and O atom penetration, Si and C atoms are not removed efficiently at an O concentration of 75% (Fig. 7c). In contrast, etching at an O concentration of 25% generates more C-C bonds than other conditions (Fig. 7a). The formation of too many C-C bonds is a much of a problem for etching at an O concentration of 25% as with the etching without O atoms (Fig. 2). However, at high O concentrations, the penetration of irradiated atoms and the generation of C-C and Si-Si bonds are observed, which prevents the removal of both Si and C atoms. To remove Si and C atoms effectively, there is a better range of O concentrations.

Next, we calculate the number of bonds during SiC etching with SF_5 and O radicals/atoms at different O concentrations to reveal the effect of O addition on bond generation in the SiC structure. Figs. 8a and b show the number of C-C and Si-Si, and Si-F, Si-O, C-F, and C-O bonds after SiC etching simulations as a function of O concentration. In addition, the results of the etching simulation without O atoms (Fig. 2) are shown as an O concentration of 0%. The data for the five simulation runs are averaged, and the error bars are also shown. Figure 8a shows that the number of Si-Si bonds is small at O concentrations of 0–60%. At these concentrations, Si atoms are likely to generate SiF_x and SiS, which prevents the Si atoms from generating Si-Si bonds. However, the number of C-C bonds is 25 at an O concentration of 0%. The number decreases to 11 as the O concentration increases from 0% to 60%. These results show that Si and C atoms are efficiently removed from the SiC surface when there are many O atoms. However, at a concentration of 75%, the number of Si-Si bonds increases to 11. The number of C-C bonds is 11 and 15 at concentrations of 60% and 75%, respectively. These are because there are fewer S and F atoms to terminate the dangling bonds of dissociated Si and C atoms at high O concentrations. This is strongly related to the kinetics on the SiC surface. The Si-Si and C-C bonds are generated by rapid bonding between dissociated Si and C atoms compared with termination of Si and C atoms by the irradiated S, F, and O atoms. The kinetics cannot be elucidated via static first-principles calculations. The understanding both the dynamics and electronic state is important to clarify etching mechanisms. Therefore, our TB-QCMD etching simulator is a powerful tool for investigating chemical reactions dynamics during etching. Etching at O concentrations of 50–60% removes Si and C atoms without generating C-C and Si-Si bonds and achieves efficient SiC etching.

To compare the chemical reactions between the dominant etchant F and O atoms, and the surface Si and C atoms, the number of Si-F, Si-

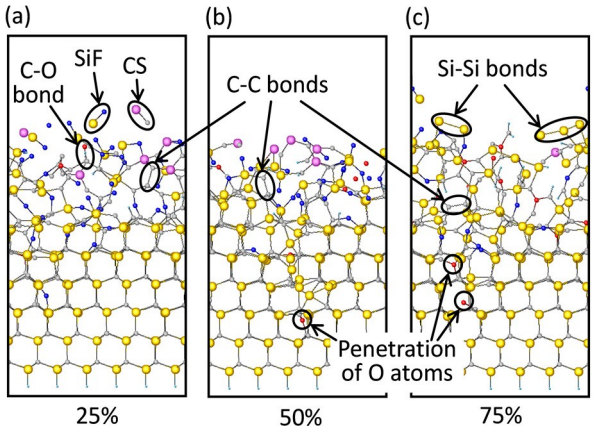

Figure 7. Snapshots of SiC etching with SF_5 and O radicals at O radical concentrations of (a) 25%, (b) 50%, and (c) 75% at 12.30 ps. The SiC surfaces are irradiated with 20 etchant species.

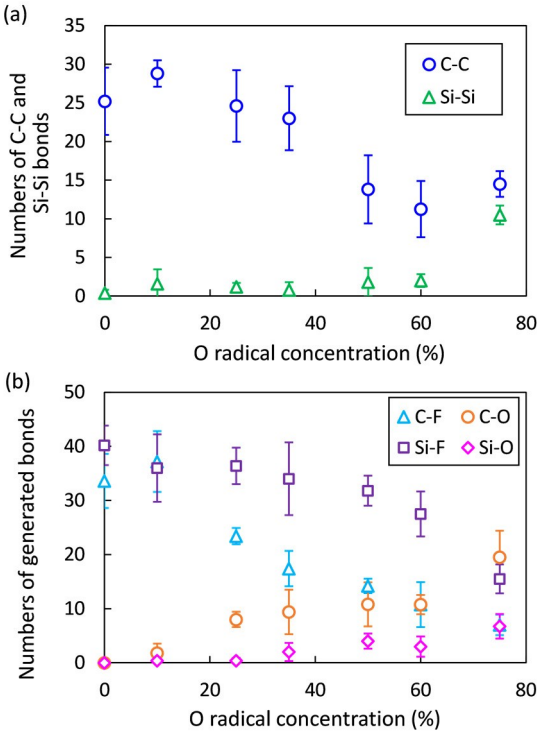

Figure 8. Number of (a) C-C and Si-Si bonds, (b) Si-F, Si-O, C-F, and C-O bonds after 20 etchant irradiations as a function of the O radical concentration during SiC etching with SF_5 and O radicals. Data are shown as averages of five simulation runs, and error bars indicate standard deviation.

O, C-F, and C-O bonds are calculated (Fig. 8b). At low O concentrations, Si-F and C-F bonds are mainly generated because many F atoms react with Si and C atoms on the SiC surface. As the O concentration increases, the numbers of Si-F and C-F bonds decrease. In particular, there are fewer C-F bonds than Si-F bonds. Therefore, an F atom is more likely to form a bond with a Si atom than with a C atom. In comparison to Si-O and C-O bonds, the number of these bonds increases with the O concentration. In particular, more C-O bonds than Si-O bonds are generated. The C-O bonds contribute to the generation and vaporization of etching products such as CO and CO_2 (Fig. 6c). In Fig. 8b, at an O concentration of 75%, the maximum number of Si-O bonds is generated. Si-O bonds remain on the SiC surface (Fig. 6c) because Si-O bonds generate SiO_2, which cannot evaporate. Therefore, etching at an O concentration of 75% produces fewer evaporable etching products. F and O atoms remove Si and C atoms most effectively, respectively. The SiC etching at the O concentrations of 50% and 60% removes Si and C atoms by generating etching products with F and O atoms efficiently because of the low numbers of C-C and Si-Si bonds generation. Here, we compare the O concentrations of 50% and 60% in the simulation with the experimental results. Considering that two O atoms are generated by an O_2 molecule, the O concentration of 50-60% can be simply converted to the ratio of O_2 of 33-43% to the total. In the experiments, etching by SF_6/O_2 plasma performed with the O_2 gas concentration of 20-30% shows high etching rate.[5,10] In a realistic plasma system, not all SF_6 and O_2 molecules are activated and change into etchant species. The activation probabilities of SF_6 and O_2 gases depend on etching systems and are probably different. For example, it is reported that the intensity of generated etchant O measured by the mass spectrometry system is higher than the intensity of SF_5.[5] In this case, O_2 is more likely to break to etchant species than SF_6. O_2 gas efficiently generates reactive O atoms, on the other hand, SF_6 gas inefficiently generates SF_3 or SF_5 radicals. To represent the experimental O_2 concentration of 20-30%, we should use an overestimated O_2 concentration in the simulation. The TB-QCMD simulation with the O_2 concentration of 33-43% well represents the experimental conditions of the O_2 concentration of 20-30%. To develop an efficient SiC etching process, the etchant composition is important for controlling the chemical reaction dynamics on SiC.

4. CONCLUSIONS

We simulated the etching of the SiC(000$\bar{1}$) surface with SF_5, SF_3, and O radicals/atoms at an irradiation energy of 300 eV by using our TB-QCMD etching simulator. During etching with SF_5 radicals, many Si-C bonds are dissociated, and SiF_x and CF_x (x = 1–4) molecules are generated, which agrees with experimental results. These behaviors are also observed for etching with SF_3 radicals. However, the SF_5 radicals dissociate more Si-C bonds and etch more rapidly than SF_3 radicals. This is because a large number of F atoms forms many Si-F and C-F bonds after Si-C bonds dissociate. The F atoms react mainly with Si atoms during etching with SF_5 and SF_3 radicals. However, many C atoms remain on the SiC surface, forming C-C bonds that decrease the etching rate. The chemical reaction dynamics during SiC etching with SF_x radicals are successfully simulated.

To decrease the number of C-C bonds, etching of SiC with SF_5 and O radicals/atoms is simulated. With 10 SF_5 and 10 O radicals/atoms, O atoms form bonds with Si and C atoms, and CO molecules evaporate. The addition of O atoms decreases the number of C-C bonds generated. However, O atoms penetrate deep layers of the SiC

structure and form bonds with Si and C atoms, so they do not generate etching products at the surface. To optimize the ratio of O to SF_5 radicals and remove Si and C atoms efficiently, we simulated SiC etching at O concentrations from 0% to 75%. The number of C-C bonds decreases as the O concentration increases from 0% to 60%. Hence, the addition of O atoms contributes to a high etching rate. However, at O concentrations of 75%, many O atoms penetrate the SiC structure, and more Si-Si and C-C bonds are generated than at concentrations of 60%. An O atom terminates only one or two dangling bonds, whereas a SF_5 radical terminates more than five. As the O concentration increases, the number of SF_5 radicals decreases. Therefore, at an O concentration of 75%, fewer dangling bonds of dissociated Si and C atoms are terminated than that at low O concentrations. The dissociated Si and C atoms form bonds with other Si and C atoms that have a dangling bond before they can be terminated by the irradiated S, F, or O atoms. Analysis of bond formations indicates that the etching processes at O concentrations of 50–60% prevent the generation of Si-Si and C-C bonds and increases the efficiency of the etching process.

The TB-QCMD etching simulation reveals the chemical reaction dynamics and etching mechanisms in SF_6/O_2 plasma. This is the first study that simulates SiC etching with two etching species by using the quantum chemical MD method, and indicates the optimal composition of etchant species. During a realistic etching system, etchant species not only SF_3, SF_5, and O but also other SF_x can cause further chemical reactions. Moreover, intermediately generated etching products such as SiF_x, CF_x, CO_y, etc. are possible to cause further reactions on the SiC surface. Namely, for the development of the SiC etching technique, those additional effects on the etching mechanism and progress are better to be investigated in the near future. Moreover, the formation process and mechanism of carbon products on the SiC by remaining C atoms are the beneficial topics to understand surface conditions during and after the SiC etching. Those are the future works for the SiC etching simulations. We hope that simulation technique improves further understanding of etching processes in the near future.

REFERENCES

1 C. A. Zorman and R. J. Parro, *Phys. Stat. Sol. b,* 2008, **245**, 1404-1424.

2 P. H. Yih, V. Saxena and A. J. Steckl, *Phys. Stat. Sol. b,* 1997, **202**, 605-642.

3 S. H. Kuah and P. C. Wood, *J. Vac. Sci. Technol. A,* 2005, **23**, 947-952.

4 Y.-H. Tseng and B.-Y. Tsui, *J. Vac. Sci. Technol. A,* 2014, **32**, 031601/1-7.

5 M. A. Fraga, R. S. Pessoa, M. Massi, H. S. Masiel and S. G. Dos Santos Filho, *ECS Trans.,* 2007, **9**, 227-234.

6 R. J. Belen, S. Gomez, D. Cooperberg, M. Kiehlbauch and E. S. Aydil, *J. Vac. Sci. Technol. A,* 2005, **23**, 1430-1439.

7 G. F. McLane and J. R. Flemish, *Appl. Phys. Lett.,* 1996, **68**, 3755-3757.

8 L. Jiang, R. Cheung, R. Brown and A. Mount, *J. Appl. Phys.,* 2003, **93**, 1376-1383.

9 N. Okamoto, *J. Vac. Sci. Technol. A,* 2009, **27**, 456-460.

10 N. O. V. Plank, M. A. Blauw, E. W. J. M. van der Drift and R. Cheung, *J. Phys. D: Appl. Phys.,* 2003, **36**, 482-487.

11 J. H. Choi, L. Latu-Romain, E. Bano, F. Dhalluin, T. Chevolleau and T. Baron, *J. Phys. D: Appl. Phys.,* 2012, **45**, 235204/1-9.

12 S. Tanaka, K. Rajanna, T. Abe and M. Esashi, *J. Vac. Sci. Technol. B,* 2001, **19**, 2173-2176.

13 W.-S. Pan and A. J. Steckl, *J. Electrochem. Soc.,* 1990, **137**, 212-220.

14 A. R. Oliveira and M. N. P. Carreno, *J. Non. Cryst.,* 2006, **352**, 1392-1397.

15 P. Chabert, *J. Vac. Sci. Technol. B,* 2001, **19**, 1339-1345.

16 X. Lu, J. Ning, Y. Qin, Q. Qiu, Z. Chuanwu, Y. Ying, J. Ming and F. Gou, *Nucl. Instrum. Meth. Phys. Res. B*, 2009, **267**, 3235-3237.

17 F. Gou, M. C. Liang, Z. Chen and Q. Qian, *Appl. Surf. Sci.,* 2007, **253**, 8743-8748.

18 A.-P. Prskalo, S. Schmauder, C. Ziebert, J. Ye and S. Ulrich, *Surf. Coat. Technol.,* 2010, **204**, 2081-2084.

19 P. V. Bui, K. Inagaki, Y. Sano, K. Yamauchi and Y. Morikawa, *Curr. Appl. Phys.,* 2012, **12**, S42-S46.

20 K. Hayashi, K. Tezuka, N. Ozawa, T. Shimazaki, K. Adachi and M. Kubo, *J. Phys. Chem. C,* 2011, **115**, 22981-22986.

21 T. Kuwahara, H. Ito, Y. Higuchi, N. Ozawa and M. Kubo, *J. Phys. Chem. C,* 2012, **116**, 12525-12531.

22 T. Kuwahara, H. Ito, K. Kawaguchi, Y. Higuchi, N. Ozawa and M. Kubo, *J. Phys. Chem. C,* 2013, **117**, 15602-15614.

23 T. Kuwahara, H. Ito, K. Kawaguchi, Y. Higuchi, N. Ozawa and M. Kubo, *Sci. Rep.,* 2015, **5**, 9052/1-7.

24 M. Elanany, P. Selvam, T. Yokosuka, S. Takami, M. Kubo, A. Imamura and A. Miyamoto, *J. Phys. Chem. B,* 2003, **107**, 1518-1524.

25 Md. K. Alam, A. Farouq, K. Nakamura, A. Suzuki, R. Sahnoun, H. Tsuboi, M. Koyama, N. Hatakeyama, A. Endou, H. Takaba, C. A. Del Carpio, M. Kubo and A. Miyamoto, *J. Phys. Chem. C,* 2009, **113**, 7723-7727.

26 H. Ito, T. Kuwahawa, Y. Higuchi, N. Ozawa, S. Samukawa and M. Kubo, *Jpn. J. Appl. Phys.,* 2013, **52**, 026502/1-9.

27 H. Ito, T. Kuwahawa, K. Kawaguchi, Y. Higuchi, N. Ozawa, S. Samukawa and M. Kubo, *J. Phys. Chem. C,* 2014, **118**, 21580-21588.

28 K. Sasata, T. Yokosuka, H. Kurokawa, S. Takami, M. Kubo, A. Imamura, T. Shinmura, M. Kanoh, P. Selvam and A. Miyamoto, *Jpn. J. Appl. Phys.,* 2003, **42**, 1859-1864.

29 M. Koyama, J. Hayakawa, T. Onodera, K. Ito, H. Tsuboi, A. Endou, M. Kubo, C. A. D. Carpio and A. Miyamoto, *J. Phys. Chem. B,* 2006, **110**, 17507-17511.

30 F. Ahmed, M. K. Alam, A. Suzuki, M. Koyama, H. Tsuboi, N. Hatakeyama, A. Endou, H. Takaba, C. A. D. Carpio, M. Kubo and A. Miyamoto, *J. Phys. Chem. C,* 2009, **113**, 15676-15683.

31 T. Onodera, Y. Morita, A. Suzuki, M. Koyama, H. Tsuboi, N. Hatakeyama, A. Endou, H. Takaba, M. Kubo, F. Dassenoy, C. Minfray, L. Joly-Pottuz, J.-M. Martin and A. Miyamoto, *J. Phys. Chem. B,* 2009, **113**, 16526-16536.

32 D. J. Oostra, A. Haring, A. E. De Vries, F. H. M. Sanders and G. N. A. Van Veen, *Nucl. Instrum. Meth. Phys. Res. B*, 1986, **13**, 556-560.
33 R. Hoffmann, *J. Chem. Phys.,* 1963, **39**, 1397-1412.
34 A. B. Anderson, *J. Chem. Phys.,* 1975, **62**, 1187-1188.
35 G. Calzaferri, L. Forss, and I. Kamber, *J. Phys. Chem.,* 1989, **93**, 5366-5371.
36 E. Emsley, *The Elements, 3rd ed.*, Oxford University Press, U.K., 1998.
37 R. S. Mulliken, *J. Chem. Phys.,* 1955, **23**, 1833-1840.
38 O. Oda, *Compound Semiconductor Bulk Materials and Characterizations*, vol. 2, World Scientific Publishing, London, 2012.
39 L. Verlet, *Phys. Rev.,* 1967, **159**, 98-103.
40 P. P. Ewald, *Ann. Phys.,* 1921, **64**, 253-287.
41 M. A. Lieberman and A. J. Jichtenberg, *Principles of Plasma Discharges and Materials Processing, 2nd ed.*, Wiley & Sons, New Jersey, 2005.
42 H. D. Hagstrum, *Phys. Rev.,* 1961, **122**, 83-113.
43 S. Rauf, T. Sparks, P. L. G. Ventzek, V. V. Smirnov, A. V. Stengach, K. G. Gaynullin and V. A. Pavlovsky, *J. Appl. Phys.,* 2007, **101**, 033308/1–9.
44 J. J. Vegh and D. B. Graves, *Plasma Source Sci. Technol.,* 2010, **19**, 045005/1–7.
45 E. A. Edelberg, A. Perry, N. Benjamin, and E. S. Aydil, *J. Vac. Sci. Technol. A,* 1999, **17**, 506-516.
46 N. Nakazaki, Y. Takao, K. Eriguchi, and K. Ono, *J. Appl. Phys.*, 2015, **118**, 233304/1-18.
47 V. Presser, M. Heon, and Y. Gogotsi, *Adv. Funct. Mater.*, 2011, **21**, 810-833.
48 Y. Wang, X. Gao, H.-J. Qui, Y. Ohta, X. Wu, G. Eres, K. Morokuma, and S. Irle, *Carbon*, 2014, **22**, 22-37.
49 B. Delley, *J. Chem. Phys*., 2000, **113**, 7756-7764.